

1 **Role of E6 in maintaining the basal cell reservoir during productive**
2 **papillomavirus infection**

3

4 Taylor Saunders-Wood¹, Nagayasu Egawa¹, Ke Zheng¹, Alberto Giarretta², Heather Griffin¹,
5 John Doorbar¹

6

7 ¹Department of Pathology, University of Cambridge, Cambridge, United Kingdom

8 ²Department of Information Engineering, University of Padova, Padova, Italy

9

10

11 Taylor Saunders-Wood and Nagayasu Egawa contributed equally to this work. Author order was
12 determined by drawing straws.

13

14 **Corresponding author:** John Doorbar, jd121@cam.ac.uk; Tel, +44 (0)1223 333734; Fax, +44
15 (0)1223 333346

16

17 Running Title: Papillomavirus lesion formation and maintenance

18

19

20 **Word count for the abstract: 224**

21 **Word count for the text: 7375**

22 **Abstract**

23 Papillomaviruses exclusively infect stratified epithelial tissues and cause chronic infections. To
24 achieve this, infected cells must remain in the epithelial basal layer alongside their uninfected
25 neighbours for years or even decades. To examine how papillomaviruses achieve this, we used the *in*
26 *vivo* MmuPV1 model of lesion formation and persistence. During early lesion formation, an increased
27 cell density in the basal layer, as well as a delay in the infected cells commitment to differentiation
28 was apparent in cells expressing MmuPV1 E6/E7 RNA. Using cell culture models, keratinocytes
29 exogenously expressing MmuPV1 E6, but not E7, recapitulated this delay in differentiation post-
30 confluence and also grew to a significantly higher density. Cell competition assays further showed
31 that MmuPV1 E6 expression led to a preferential persistence of the cell in the first layer, with control
32 cells accumulating almost exclusively in the second layer. Interestingly, the disruption of MmuPV1
33 E6 binding to MAML1 protein abrogated these phenotypes. This suggests that the interaction between
34 MAML1 and E6 is necessary for the lower (basal) layer persistence of MmuPV1 E6 expressing cells.
35 Our results indicate a role for E6 in lesion establishment by facilitating the persistence of infected
36 cells in the epithelial basal layer; a mechanism that is most likely shared by other papillomavirus
37 types. Interruption of this interaction is predicted to impede persistent papillomavirus infection and
38 consequently provides a novel treatment target.

39

40 **Importance**

41 Persistent infection with high-risk HPV types can lead to development of HPV-associated cancers,
42 and persistent low-risk HPV infection causes problematic diseases, such as recurrent respiratory
43 papillomatosis. The management and treatment of these conditions poses a considerable economic
44 burden. Maintaining a reservoir of infected cells in the basal layer of the epithelium is critical for the
45 persistence of infection in the host, and our studies using the mouse papillomavirus model suggest
46 that E6 gene expression leads to the preferential persistence of epithelial cells in the lower layers
47 during stratification. The E6 interaction with MAML1, a component of the Notch pathway, is required
48 for this phenotype, and is linked to E6 effects on cell density and differentiation. These observations
49 are likely to reflect a common E6 role that is preserved amongst papillomaviruses, and provide us
50 with a novel therapeutic target for the treatment of recalcitrant lesions.

51

52 **Introduction**

53 Papillomaviruses (PV) are small, non-enveloped, double-stranded DNA tumour viruses that infect
54 more than 80 different species. Over 405 papillomavirus genomes are currently listed in the
55 Papillomavirus Episteme (<http://pave.niaid.nih.gov>), of which 198 infect humans. PVs have a
56 common genome organisation, and encode ‘core’ proteins required for viral genome replication and
57 packaging (i.e. E1, E2, L1 and L2), along with a number of more divergent ‘accessory proteins’, such
58 as E6 and E7, which modify the infected cell to allow replication and persistence. In high-risk PVs,
59 E6 and E7 are considered as oncogenes, and are important in the development of PV-associated
60 cancers. The majority of PVs are, however, classified as low-risk, and are associated only with benign
61 papillomas or inapparent infections (1). PV evolution and diversification has been impacted by the
62 colonisation of specific epithelial niches, with co-evolution and niche adaptation allowing PVs to
63 develop their remarkable species and tissue specificity (2). Although papillomavirus protein functions
64 may vary between PV species and types, as a group they share common life cycle strategies, including
65 the need to persist in the epithelial basal layer following infection. In this context, animal models of
66 infection have proven useful in establishing many of the basic principles that control how
67 papillomavirus lesions form and how productive infection is regulated by viral gene products.

68 Until recently, the field has lacked a PV that can infect and be propagated in laboratory mice.
69 MmuPV1 (originally MusPV (3)), a member of the pi papillomavirus genus, was isolated in 2011
70 from cutaneous lesions (4), with subsequent research demonstrating an additional ability to infect a
71 range of mucosal sites (5-7). Although generally considered as a model of human beta papillomavirus
72 infections, it has also been used to study PV carcinogenesis at the female reproductive tract, a site
73 which is targeted in humans by the high-risk alpha papillomaviruses (8). The availability of MmuPV1
74 provides an opportunity to model many fundamental principles of PV infection, and to develop a
75 broader understanding of PV biology and disease pathogenesis (9-13).

76 Human papillomaviruses (HPVs) are split into five genera based on nucleic acid sequence divergence
77 with high-risk alpha PVs causing a range of human cancers (14). Low-risk alpha papillomaviruses
78 generally cause benign warts, with beta and gamma types typically associated with only persistent
79 asymptomatic infections in immunocompetent individuals (1). Although beta PVs are part of the

80 normal commensal microbial flora (15), they can cause cutaneous squamous cell carcinoma (cSCC) in
81 patients suffering from epidermodysplasia verruciformis (EV) (16, 17). PV infection typically occurs
82 following a microwound, which allows virus particles to access the mitotically active basal cells on
83 the basal lamina (reviewed in (18)), which are responsible for the maintenance and replenishment of
84 all layers of the skin.

85 To maintain epithelial homeostasis, the loss of cells from the basal layer must be precisely matched by
86 basal cell division, which is considered to be mediated by discrete groups of slow-cycling stem cells
87 that maintain progeny transit-amplifying cells, to produce epidermal proliferative units (EPU) (19,
88 20). Lineage tracing data has, however, suggested that the epithelium may alternatively be maintained
89 by committed progenitor cells, and that individual cell fate is determined at random (21, 22). It has
90 been suggested that PV could modulate the infected cell, giving it stem-like properties, such as
91 upregulation of stem cell marker genes or delayed differentiation as a result of the inhibition of the
92 Notch signalling pathway (23-25). In such ways, keratinocytes infected with PV may develop stem-
93 like traits following an infection. Understanding this element of basal cell homeostasis during early
94 papillomavirus lesion formation and persistence appears to be important in the development of
95 therapeutics targeting the persistently infected basal cell.

96 Although unclear, it is plausible that only one single infected cell is enough to establish a new lesion.
97 Therefore, understanding what competitive advantages such a cell must have in order to develop a
98 lesion, and how it can persist in the basal layer, is important; ascertaining the way in which single
99 infected cells compete with uninfected neighbours to form lesions could reveal key mechanisms of
100 infection. These mechanisms may also explain how certain HPV types can establish productive
101 lesions without the pro-proliferative capabilities of their high-risk counterparts. Both *in vivo* and *in*
102 *vitro*, Notch signalling has been shown to act as a key determinant in the coordination of keratinocyte
103 transition from proliferation to early-stage differentiation phenotypes (26). Inactivation studies have
104 demonstrated the role of Notch signalling in regulation of late-stage differentiation in keratinocytes
105 (27). Other studies have also shown the involvement of Notch signalling in the differentiation process
106 (26, 28). Notch signalling plays a vital role in successful maintenance of keratinocytes in normal
107 epithelium; given the previously discussed ability of PVs to interact with this pathway, it is clear that

108 Notch pathway interaction could be implicated in PV modulation of the cell to successfully persist in
109 hosts.

110 Here, we study the characteristics of infected cells with a view to understand how infections develop
111 and persist, by examining and modelling the generic characteristics of PV infection using the mouse
112 model of papillomavirus infection. Given the broader life cycle strategies shared by all PV types,
113 MmuPV1 provides a useful model with which to study aspects of persistence and cell competition *in*
114 *vivo* by examining the mechanics of basal cell expansion. We have identified four key stages during
115 papillomavirus lesion formation. A delay in differentiation and an increase in cell density are early
116 viral modifications during this process. As lesions become established, a weak bimodality in E6/E7
117 expression becomes apparent in infected basal cells, with higher expression levels correlating with
118 delamination, migration into the parabasal cell layers in the absence of accompanying differentiation,
119 and the induction of K10 expression. Our results suggest that E6 is responsible for these phenotypic
120 changes, with the protein conferring a preferential advantage over neighbouring uninfected cells,
121 which, in *in vitro* assays, are displaced into the stratified cell layers. This competitive advantage,
122 which is mediated in part through modulation of the Notch pathway, points to an important role for E6
123 in establishing and maintain the reservoir of papillomavirus infection in the epithelial basal layer.

124

125 **Results**

126 **Stages of papillomavirus lesion formation in immunodeficient and immunocompetent mice**

127 Our previous report showed that early visible lesion formation can be observed at day 6 or 7 post-
128 inoculation of high-titre viruses (29). To observe the process of lesion formation, nude mice were
129 scarified at three discrete regions along the tail, and approximately 2×10^9 VGE MmuPV1 cell-free
130 virus was introduced at each site. To identify the earliest stages of lesion formation, mouse tails were
131 collected between days one and five post-inoculation. When lesions became macroscopically visible
132 (early visible) at any site on day 6 or 7 post-inoculation, the entire tail was collected, allowing the
133 identification of 'pre-visible' lesions present elsewhere on the same tail. The well-established lesions
134 (warts) were also collected 10-14 days post-inoculation. In Figure 1, four discrete stages of lesion
135 formation are shown.

136 Stage one depicts the earliest detectable lesion events (Figure 1A). Of the genes examined, only
137 expression of E6/E7 could be detected, which was restricted to a subset of basal and parabasal cells
138 and was apparent as early as day two post-inoculation. Among the 48 samples collected, E6/E7
139 expression was only seen in regions where re-epithelialisation was complete, suggesting that the early
140 stages of wound healing must be completed before viral gene expression begins. In stage two (Figure
141 1B), the first evidence of MmuPV1 virus production is apparent in the uppermost layers, shown by
142 the expression of viral capsid protein, suggesting the development of productive lesions without
143 macroscopic/visible change. Additional discrete foci of infection (red dotted lines) became apparent as
144 lesion development progressed, suggesting that larger lesions develop from multiple discrete foci
145 which coalesce to form one lesion. In stage three (Figure 1C), the lesion becomes macroscopically
146 visible for the first time. We observed high basal cell density at the lesion site, as seen throughout the
147 basal layer of the example shown, and referred to here as 'early visible lesions'. In this example, one
148 continuous region of infection has developed, apparently from multiple foci visible at the previous
149 stage. Finally, in stage four of lesion formation, we see induction of papillomatosis and warts
150 macroscopically, subsequently referred to here as 'established lesions'.

151 Infection of C57BL/6 immunocompetent mice with MmuPV1 inoculation did not result in the
152 formation of papillomas at the tail sites, which is in contrast to the macroscopically visible lesions that

153 form in nude mice (Figure 2A). A thorough analysis of tissue samples led to the identification of
154 productive microlesions in the C57BL/6 mouse tail tissue at the site of infection at ten days post-
155 inoculation (Figure 2B). As shown in Figure 2B(i), expression of E6/E7 RNA was evident in the
156 epithelial basal cells and persisted into the upper layers of the epidermis towards the skin surface. This
157 prominent cytoplasmic distribution of virus transcripts differs from the less clearly defined basal
158 expression seen in our athymic nude immunodeficient model, which was predominantly nuclear.
159 Similarly, the E4 protein can be seen co-localising to this area, confirming the presence of a PV-
160 induced microlesion. Finally, immunofluorescent staining identified the presence of occasional L1-
161 expressing cells in the upper layers, which suggests the development of a productive lesion (Figure
162 2B(i)). Figure 2B(ii) shows a second example of a lesion located at a wound site seven days post-
163 wounding. Whilst E6/E7 RNA and E4 protein are also both present at this site, L1 could not be
164 located. Therefore these lesions in the immune competent animals are understood to have reached
165 stage 2 of lesion formation.

166

167 **MmuPV1 modulation of post-infection basal cell density**

168 An apparent correlation between the appearance of E6/E7 RNA expression and increase in basal cell
169 density was observed from stage two of lesion formation onwards. Since this phenotype was seen
170 early during lesion formation in the basal layer, involvement of a viral early protein was suspected. To
171 examine this further, a more quantitative analysis was carried out, with uninfected and mock-infected
172 epithelium serving as controls. Two time points during lesion formation were examined in order to
173 establish basic principles: ‘early visible lesions’, which are equivalent to stage 3 during lesion
174 formation (Figure 1C), and ‘established lesions’, which are florid tail lesions collected more than 10
175 days post-infection (Figure 1D). For the early visible lesion analysis, macroscopically visible lesions
176 that were collected 6- or 7-days following virus inoculation, and which were shown to express viral
177 E4 proteins (or E6/E7 RNA analysis), were used (Figure 3A). Time-matched mock-infected sites,
178 which were shown to express reepithelialisation Keratin 17 (Figure 3A)(30), were selected for
179 comparison with the early visible lesions. For quantification, 40 image sets of DAPI stained tissue
180 were collected for each category (i.e. uninfected epithelium, mock wound site, early visible lesions

181 and established lesions (mice n=4 per group)), and basal cell number was counted in 450 μm stretches
182 in each image (red lines in Figure 3A). Basal cell density was found to be elevated in early-visible
183 lesions when compared to all other categories, and averaged 0.22 cells per μm ($p \leq 0.01$; see Figure
184 3B). By contrast, uninfected epithelium and mock wound sites averaged 0.18 and 0.16 basal cells per
185 μm respectively, with basal cell density at uninfected epithelial sites being similar to that observed in
186 established lesions (0.16 cells per μm).

187 To investigate this phenomenon in more detail, we proceeded to establish if the number of cells driven
188 to replicate their DNA was altered in the virus infected basal cells, and whether this differed between
189 early visible and established lesions. Bromodeoxyuridine (BrdU) incorporation was monitored by
190 collecting tissue samples 24 hours after intraperitoneal injection of BrdU by immunofluorescence
191 (Figure 3C), and the proportion of BrdU-positive basal cells in uninfected epithelium, mock wound,
192 early visible lesions, and established lesions was established. A statistically significant increase in the
193 proportion of BrdU positive cells in the basal layer in the stage five/early visible lesion was apparent
194 when compared to uninfected epithelium (Figure 3D). In both uninfected tail epithelium and mock
195 infected tail sites, approximately 14% and 13% of basal cells were BrdU positive respectively, with no
196 significant difference apparent between the two groups. In the early visible lesions, 25% of cells in the
197 basal layer were positive for BrdU following our labelling regime. There was no significant difference
198 in percentage of BrdU positive basal cells between early visible lesions and established lesions, in
199 which 24% of basal cells were positive for BrdU. The percentage of BrdU positive cells in early
200 visible and established lesions was significantly higher than in both uninfected epithelium and mock
201 wounded epithelium ($p < 0.01$). Although the percentage of BrdU positive cells may be expected to
202 differ between mock infected and uninfected epithelium, re-epithelialisation has been largely
203 completed at this point, and the percentage of replication competent cells that become labelled during
204 24 hours period is similar. These results suggest that the elevated basal cell density observed in early
205 visible lesions is unlikely to be a consequence of inherent differences in cell cycle progression and
206 proliferation, prompting us to look at viral gene expression in relation to basal cell retention and
207 differentiation.

208

209 **E6/E7 expression correlates with a delay in normal differentiation in the parabasal layers of**
210 **infected epithelium**

211 As the above analysis suggests that an increase in basal cell density could not be attributed to
212 increased cell replication alone, it was postulated that MmuPV1 E6/E7 expression may lead to
213 persistence of infected cells in the basal layer by overcoming normal cell density modulation and
214 contact inhibition. To investigate this in our time course of lesion formation, the expression level of
215 E6/E7 RNA in individual cells was evaluated in the basal cell layers across stage three, early visible
216 lesions. Following quantification of the level of E6/E7 RNA (Figures 4A and B), a weak bimodality
217 was apparent in E6/E7 RNA expression levels of the basal cells, suggesting the presence of two
218 discrete cell populations, with the majority expressing these viral genes at a low level. Although a test
219 of bimodality did not confirm statistical significance (Hartigan's dip test, $p=0.914$), the data was
220 significantly not normal when all three normality tests were applied (D'Agostino & Pearson normality
221 test, $p<0.0001$; Shapiro Wilk normality test, $p<0.0001$; KS normality test, $p<0.0001$). The sum of
222 two Lorentzian curves (shown in red on histogram in Figure 4B) closely fitted our observational data.
223 To examine the involvement of E6/E7 RNA expression in basal cell exit and differentiation, two
224 markers of epithelial differentiation were used; K10, an established early-stage marker of cells
225 entering terminal differentiation, and HES1, a downstream target of the Notch signalling pathway
226 (28), which is also known to be a target of MmuPV E6 (25). Double staining for MmuPV1 E6/E7
227 RNA and K10 demonstrated that in the presence of the early MmuPV1 E6/E7 RNA, K10 is
228 completely absent (Figure 5A) in the second layer. Expression of HES1 RNA was not noticeably
229 delayed in these areas of delayed differentiation when compared to surrounding normal epithelium,
230 and was expressed throughout the basal and parabasal layers (Figure 5B). As seen in the experiments
231 carried out with immunodeficient mice, there is also a decrease in K10 staining that correlates with
232 the elevated HES1 phenotype present in immunocompetent microlesions (Figure 5C). In fact,
233 quantification of HES1 RNA expression per cell in the basal layer of lesions versus uninfected tissue
234 demonstrated a significantly higher level of HES1 RNA expression in the infected basal cells (Figures
235 5D and E), suggesting that while differentiation was retarded, the Notch signalling pathway was

236 active. Therefore, it is not total inhibition of the Notch pathway by E6/E7 that leads to the observed
237 delay in differentiation, where cells exited the basal layer without differentiating. This data indicated
238 that in both immunocompetent and immunosuppressed backgrounds, MmuPV1 infection delayed
239 differentiation commitment in the basal and parabasal layers, which we suspect will enhance basal
240 layer-persistence of the infected cell. E6 has previously been speculated to regulate commitment to
241 differentiation (24), therefore it was decided that examination of this phenotype in a cell culture model
242 wherein individual protein functions can be discretely analysed would be carried out.

243

244 **Keratinocytes expressing MmuPV1 E6, but not E7, show higher saturation density in 2D culture**

245 To overcome some of the complexities encountered in *in vivo* experiments, cell culture systems were
246 introduced to add clarity and to further explore our emerging hypotheses. To determine which of the
247 viral proteins confers the *in vivo* cell density and differentiation phenotypes observed, Normal
248 Immortalised Keratinocyte (NIKS) cell lines exogenously expressing MmuPV1 E6 (NIKS/LXSN-
249 MmuPV1E6) or MmuPV1 E7 (NIKS/LXSN-MmuPV1E7) were generated. NIKS containing an
250 empty LXSN vector were used as a control (NIKS/LXSN).

251 As an increase in cell density and cell proliferation had been quantified *in vivo*, 2D monolayer growth
252 assays were carried out to establish the role of each protein *in vitro* (Figure 6A). From days one to
253 three, before cells had reached confluence, there was no significant difference in the growth rate of
254 cells across all three groups. After cells had reached confluence (day 4-6), the increase in cell counts
255 of NIKS/LXSN and NIKS/LXSN-MmuPV1 E7 plateaued, and at day 7, there was no significant
256 difference, 1.55×10^6 and 1.53×10^6 cells respectively. In contrast, NIKS/LXSN-MmuPV1E6 cells
257 reached 3.1×10^6 , a significantly higher density when compared to the other two groups
258 (**** $p \leq 0.0001$), demonstrating that MmuPV1 E6 plays an important role in maintaining the
259 proliferative capacity of the cell as cell density increases.

260 As shown in Figure 6B, the morphological appearance of the NIKS/LXSN and NIKS/LXSN-
261 MmuPV1E7 cells by day 7 were highly differentiated (shown with red arrows), whereas in
262 NIKS/LXSN-MmuPV1E6 cells the small, bright, rounded cells are indicative of cells still undergoing
263 replication (denoted with black arrows). Analysis of K10 staining in all three populations indicated

264 that at low densities almost all cells lacked K10. However, at high density, while NIKS/LXSN and
265 NIKS/LXSN-MmuPV1E7 cells showed a similar level of K10 expression per field,
266 NIKS/MmuPV1E6-LXSN cells had noticeably lower expression levels of K10. Quantification
267 analysis showed that when data was normalised by the total number of cells per field to calculate the
268 percentage of positive cells per field, there was a statistically significant decrease in the percentage of
269 K10 positive cells per field (** $p \leq 0.01$) in NIKS/MmuPV1E6-LXSN cells when compared to the
270 other two groups (Figure 6C). This shows that the effect of MmuPV1 on differentiation seen *in vivo* is
271 also seen in the cell culture model, and that MmuPV1 E6 is responsible for this phenotypic change.

272

273 **Keratinocytes expressing MmuPV1 E6, but not E7 persist in the ‘lower’ layer of cells in a high** 274 **cell density culture environment**

275 Thus far, our work implicates MmuPV1 E6 in the differentiation delay and increased cell density
276 observed in our *in vivo* model. As our results suggested that increased cell proliferation was not
277 responsible for the observed increase in cell density (Figure 3), we wanted to investigate the idea that
278 preferential persistence of infected cells in the basal layer could lead to the increased density observed
279 as lesions first begin to form. To investigate this, we established NIKS/LXSN, NIKS/LXSN-
280 MmuPV1E6-LXSN and NIKS/LXSN-MmuPV1E7 expressing eGFP or mCherry to observe their
281 relative cell growth characteristics over time by culturing them together to produce a cell competition
282 assay system. In this assay, at the start the two cell types were seeded at the same high density to
283 overcome the difference in expansion growth characteristics of each cell line, so that the different cell
284 populations grew from confluence onwards. In this culture condition, NIKS cells start to express K10
285 in second-layer cells only but K14 in both layers (Figure 7A). The expression pattern is observed in
286 organotypic raft culture tissue of NIKS(24). This competition assay system provides a crude model of
287 a confluent basal layer; cells in this culture are confluent with no space to grow, which is the same
288 spatial environment in which basal cells naturally exist. For each well, half of the population seeded
289 were NIKS/QCXIP-eGFP/LXSN cells, the other half being NIKS/QCXIP-mCherry/LXSN,
290 NIKS/QCXIP-mCherry/LXSN-MmuPV1E6 or NIKS/QCXIP-mCherry/LXSN-MmuPV1E7. Cells
291 were cultured for up to 10 days, with the growth of these mixed cell populations observed by confocal

292 microscopy. At day one (Figure 7B), all three experimental groups had an approximate 50:50 ratio of
293 red versus green cells, as expected. A slight increase in red cells in both the NIKS/QCXIP-
294 eGFP/LXSN cells versus NIKS/QCXIP-mCherry/LXSN-MmuPV1E6 cells (LXSN/LXSN-
295 MmuPV1E6) group and the NIKS/QCXIP-eGFP/LXSN cells versus NIKS/QCXIP-mCherry/LXSN-
296 MmuPV1E7 (LXSN/LXSN-MmuPV1E7) group was apparent, and although not statistically
297 significant, suggests a slight advantage in cell attachment or cell growth over control cells in the first
298 24 hours. At day ten (Figure 7C and D), there were approximately 50% of each cell population
299 occupying both the lower and upper layer of cells in the NIKS/QCXIP-eGFP/LXSN versus
300 NIKS/QCXIP-mCherry/LXSN (LXSN/LXSN) group and in the LXSN/LXSN-MmuPV1E7 group.
301 Conversely, within the LXSN/LXSN-MmuPV1E6 group the vast majority of cells occupying the
302 lower layer of cells in culture were NIKS/QCXIP-mCherry/LXSN-MmuPV1E6 cells (92.6% red
303 cells), whilst the upper layer of cells consisted almost entirely of NIKS/QCXIP-eGFP/LXSN cells
304 (94.3% green cells). This suggested that NIKS expressing MmuPV1E6 were preferentially persisting
305 in the lower layer of cells. To observe these phenotypes in 3D, maximum intensity side views of
306 orthologue plots for each cell population are shown (Figure 7E). This again demonstrates that in the
307 LXSN/LXSN and LXSN/LXSN-MmuPV1E7 groups, each cell type can be seen distributed in
308 roughly equal measure in both layers. Conversely, in the LXSN/LXSN-MmuPV1E6 group, a lower
309 layer of MmuPV1E6 expressing cells can clearly be seen, whilst the upper layer consists of almost
310 exclusively LXSN control cells. Taken together, this data shows that expression of MmuPV1 E6, but
311 not E7, affords the cell a growth advantage or a capability of remaining at the bottom layer over the
312 control cell population when in direct competition for space. Actually, quantitative analysis of the
313 lower layer of cells in each of these groups was carried out at day ten (Figure 8). Data demonstrated
314 that the NIKS/LXSN-MmuPV1E6 group reached a significantly higher density in the lower layer of
315 cells when compared to the separately grown NIKS/LXSN and LXSN/LXSNMmuPV1E7. This data
316 corroborates earlier results both *in vivo* and *in vitro* demonstrating that MmuPV1 E6 expressing cells
317 can grow to higher cell densities than control cells, and also suggests that increased basal cell density
318 observed in the early mouse lesions (Figure 3A and B) is due primarily to MmuPV1 E6 expression.

319 Finally, the data could suggest that, in addition to the cell density, the rate at which cells are exiting
320 this bottom layer may be affected.

321

322 **MAML binding deficient MmuPV1 E6 loses ability to persist in the ‘lower’ layer**

323 To further understand the molecular pathways involved in directing this particular competitive
324 advantage of MmuPV1 E6-expressing cells, a mutant MmuPV1 E6 was generated. Previously
325 published research into the similarities between MmuPV1 E6 and HPV8 E6 interactions with the
326 Notch pathway confirmed that MmuPV1 E6 was able to bind to MAML, and that this interaction
327 delayed differentiation in Ca²⁺ treated keratinocytes (25). It was shown that an E6 MAML binding
328 mutant could not inhibit Notch signalling, and that this mutant was unable to form papillomas *in vivo*.
329 As such, it was postulated that this pathway may be involved in the phenotype observed in the high-
330 density competition assay, and that similar interference with MmuPV1 E6 MAML1 binding in this
331 model could indicate whether the downstream Notch signalling pathway was involved in modulation
332 of the persistence phenotype. Therefore, a MAML1 binding mutant of MmuPV1 E6, MmuPV1^{R130A},
333 was generated. Using an immunoprecipitation assay it was confirmed that the MmuPV1-E6^{R130A} had a
334 reduced ability to bind to MAML1 (Figure 9A). NIKS-expressing MmuPV1-E6^{R130A} had no
335 significant difference in cell density at day 7 when compared to LXSXN-expressing cells, unlike
336 MmuPV1-E6 expressing cells, which grew to a significantly higher density (**** $p \leq 0.0001$) by this
337 time point (Figure 9B). Furthermore, cells expressing MmuPV1-E6^{R130A} no longer showed a delay in
338 differentiation post-confluence when stained with K10 (Figure 9C). Quantification of the number of
339 K10 positive cells (Figure 9D) demonstrated that the percentage of K10 positive cells per field was
340 significantly lower in the population of NIKS/MmuPV1E6^{R130A}-LXSXN cells (** $p \leq 0.05$) when
341 compared to the other groups, suggesting that the delay in differentiation observed and quantified in
342 NIKS/LXSXN-MmuPV1E6 cells is lost upon introduction of the E6^{R130A} MAML1 binding mutation.
343 Again, the cell competition assay and layer analysis were repeated with NIKS/QCXIP-
344 mCherry/LXSXN-MmuPV1E6^{R130A} cells versus NIKS/QCXIP-eGFP/LXSXN cells (LXSXN/LXSXN-
345 MmuPV1E6^{R130A}). Results of the cell competition assay are shown in Figures 10A and B. In the
346 LXSXN/LXSXN-MmuPV1E6^{R130A} group, there was a statistically significant difference (**** $p \leq 0.0001$)

347 between layer occupancy when compared to LXS/N/LXS/N-MmuPV1E6 groups at day 10. While the
348 lower layer occupancy was 89.4% NIKS/QCXIP-mCherry/LXS/N-MmuPV1E6 cells, this was reduced
349 to 60.8% for the MAML1 NIKS/QCXIP-mCherry/MmuPV1E6^{R130A}. Similarly, the upper layer of
350 LXS/N/LXS/N-MmuPV1E6 group consisted of 93.2% EGFP positive (NIKs/PQCXIP-eGFP/LXS/N)
351 cells, whereas this decreased to only 64.5% in the LXS/N/LXS/N-MmuPV1E6^{R130A} group. This
352 phenotype is also confirmed in 3D (Z-stack image) (Figure 10C). The NIKS/LXS/N-MmuPV1E6^{R130A}
353 mutant cell line did not retain the ability of wild type E6 to persist preferentially in the lower layer,
354 instead demonstrating a random assortment of eGFP positive and mCherry positive cells in the lower
355 and upper layers (Figure 10C). Finally, quantification of cell density in the lower layer of the
356 LXS/N/LXS/N-MmuPV1E6^{R130A} group showed that the increase in lower layer density previously
357 observed in the LXS/N/LXS/N-MmuPV1E6 group (Figure 8) was also lost following the disruption of
358 MmuPV1 E6 MAML1 binding, as there was no significant difference between the LXS/N/LXS/N-
359 MmuPV1E6^{R130A} and NIKS/LXS/N groups in lower layer cell density at day ten (Figures 8 and 10D).
360 This data clearly demonstrated that MmuPV1 E6 interference with the Notch pathway via interaction
361 with MAML1 is necessary to allow cells to preferentially persist in the lower layer of cells and may
362 also mediate the effect of MmuPV1E6 on basal lower cell layer density regulation.
363

364 **Discussion**

365 Papillomaviruses exclusively infect the stratified squamous epithelium to induce chronic infection in
366 their host (31). Despite advancements in the field, the earliest events in lesion formation (infection of
367 a cell, initial stages of lesion development, and the associated molecular mechanisms), are less well
368 understood. This paper aims to investigate the initial events in lesion formation to better understand
369 how, in these first stages of infection, single infected cells can persist and outcompete uninfected
370 cells.

371 The incubation period of papillomaviruses from exposure to lesion development varies greatly, the
372 usual range being between 1 and 20 months (32). Initial events during the incubation period are still
373 unknown, and it has been proposed that co-cofactors (e.g. host/local immunity, synergistic infection,
374 inflammation or tobacco use) may be required for lesion initiation (33), and if the co-factor is not
375 present, the papillomavirus may lie in dormant/latent infection and only express itself after the co-
376 factor appears. In our previous study using the papillomavirus mouse model (29), however, the
377 incubation period in nude mice was basically determined by the virus titre inoculated. Lesions formed
378 in one week in mice inoculated with high virus titre, whereas with low titre lesion formation took 12
379 weeks. This suggested that the number of initial infection events may define how quickly the lesion
380 forms (becomes apparent). Indeed, we observed that when high titre virus was inoculated, lesions
381 initially started from multiple micro-foci of infected cells surrounded by non-infected cells. These
382 micro-foci expanded in the basal layer to form one continuous region of infected cells before
383 becoming apparent (Figure 1B). This observation supports the idea that PV infection and expression
384 of virus genes confers 'fitness' to infected cells compared with uninfected cells in their growth in the
385 epithelial basal layer, and eventually leads to elimination of non-infected cells from the lesion (34,
386 35). Interestingly, we were able to locate two microlesions in these immunocompetent mice (Figure
387 2). Whilst appearing briefly productive at both of these sites, no macroscopic lesions formed on the
388 tail, which was in agreement with previous research (36). We can infer from their rare occurrence
389 rates when compared to the immunodeficient model that these microlesions occur transiently before
390 clearance by the immune system. Or, they may occur at such small, controlled sites that they are
391 simply extremely hard to locate. In previous reports, MmuPV1 is shown to form macroscopic lesions

392 in UVB-irradiated or T-cell depleted immunocompetent mice, suggesting that T cell mediated
393 immunity is controlling macroscopic lesion formation (12, 36). In NOD/SCID mice which have a
394 deficiency in T, B, and NK cells, MmuPV1 showed only minimal disease at cutaneous sites, but
395 developed persistent infection at the mucosal sites including those of the anogenital region and the
396 oral cavity, suggesting MmuPV1 may have tissue (mucosal) preference (37). Indeed, MmuPV1
397 persistent and productive lesions have been located in the reproductive tract of FVB
398 immunocompetent mice (8). As such, the phenotype of MmuPV1 infection (incubation time,
399 macroscopic/microscopic lesion formation, clearance, persistent infection or pattern of viral gene
400 expression) also appears to be determined by co-cofactors (e.g. host/local immunity, genetic
401 backgrounds, inflammation or site of infection).

402 The viral genes of papillomaviruses are categorised as core or accessory genes (14). In general, the
403 viral core genes carry out essential functions during the virus life cycle in the epithelium, and these
404 basic functions are conserved throughout papillomaviruses. L1 encodes the primary structural protein
405 in the virus capsid, with the minor capsid protein L2 binding to the circular viral DNA to facilitate
406 optimal genome encapsidation. E1 encodes a virus-specific DNA helicase, while E2 functions in viral
407 transcription, replication and genome partitioning. In contrast, the accessory genes encode proteins
408 that modify the cellular environment. In many cases these proteins perform similar but not necessarily
409 identical functions during the life cycle of different papillomaviruses to support lesion
410 formation/maintenance, and the production of progeny virions, which are thought to determine their
411 pathogenicity. During the early steps of MmuPV1 lesion formation, papillomavirus gene expression
412 cellular phenotypes such as increased cellular density and delayed differentiation (Figures 1, 2 and 4)
413 were observed, suggesting that the infected cells have a growth advantage or remain more
414 preferentially in the basal layer compared to adjacent non-infected cells. As the expression level of
415 MmuPV1 accessory genes (E6 and E7) showed some heterogeneity and the higher expression may
416 correlate to a cellular morphology which can be characterised as cells leaving the basal layer
417 (delamination), virus genes might also be relevant to the delamination step of infected cells (Figure 4),
418 but this should be elucidated in future study. Results from keratinocytes expressing MmuPV1 E6 or
419 E7 genes showed that MmuPV1 E6 was responsible for these cellular phenotypes, not MmuPV1 E7.

420 MmuPV1 E6 appeared to inhibit contact inhibition, increase growth post-confluence resulting in
421 higher saturation density, and delay keratinocyte differentiation (Figure 6). This is similar to
422 phenotypes observed in our recently published paper, which showed exogenous expression of low-
423 risk HPV11 E6, but not E7, afforded a growth advantage and differentiation delay to keratinocytes
424 post-confluence (38), suggesting there may be similar mechanisms between mouse papillomavirus
425 and low-risk HPV types, despite their relatively distant relationship (39). In the competition assay,
426 which allows us to investigate the growth advantages of certain types of cells in mixed cell
427 populations in 3D by isolating discrete layers of cells within the monolayer culture, keratinocytes
428 expressing MmuPV1 E6 demonstrated a clear phenotype of persistence in the 'lower' layer of cells
429 when cultured with control keratinocytes, whereas expression of MmuPV1 E7 did not (Figure 7). This
430 data suggests that expression of key virus proteins in distinct locations of the cell monolayer, and so
431 possibly within the tissue, affords a cellular fitness over uninfected cells in the basal layer. Overall,
432 our results suggest that the primary functions of E6 in the viral life cycle is to maintain the infected
433 cells in the basal layer and to support lesion formation. It is plausible to suggest that E7 could function
434 in the upper layer of infected epithelial cells by driving cell cycle entry to produce pseudo-S phase
435 and supporting viral genome amplification, which must be investigated in future studies. The main
436 limitation of our *in vitro* experimental model is the use of spontaneously immortalised human
437 keratinocyte (NIKS) for evaluation of mouse papillomavirus gene function. The use of NIKS has also
438 some advantages. The isogeneity as well as non-virus-gene-dependent growth of NIKS allow us to
439 conduct comparative analysis and reproduce the data more consistently. The increased fitness of cells
440 in the propagation in the basal layer was confirmed in the competition assay using mouse primary tail
441 keratinocyte (data not shown), however further investigations should be done to elucidate how
442 papillomavirus genes of each PV have evolved their functions to maximise the fitness to each site of
443 infection (keratinocytes of the different sites of body) in future.

444 In the past two decades, signalling pathways involved in the control of keratinocyte behaviour relating
445 to epithelial tissue homeostasis have been described (40, 41). However, knowledge of the molecular
446 mechanisms by which cells respond to a given signal, such as cell density, mechanical stress, and

447 growth factors, is insufficient to explain how a specific cell might change its behaviour (proliferation
448 and commitment of differentiation), and how other surrounding cells behave differently in response.
449 Notch signalling mediates short-range signalling interactions between a cell and its neighbouring cells
450 and controls the fate of each differently. In doing so, Notch is thought to be a master regulator of
451 keratinocyte differentiation. In normal stratified epithelium, the activity of the Notch pathway is
452 spatially regulated by the preferential distribution of Notch ligands and receptors in the different
453 epidermal layers. The basal layer mainly expresses Notch ligands, in contrast, the Notch receptors are
454 enriched in the suprabasal layers where Notch signalling is considered to be most active (42, 43). The
455 Notch pathway is known to be required for the transition of keratinocytes from the basal to the
456 suprabasal layers (44). Several PV E6 proteins are also known to target Notch pathways. High-risk
457 HPV types appear to down-regulate the expression of Notch receptor via the degradation of p53(45),
458 which results in repression of differentiation markers in keratinocytes (24, 45). In contrast, cutaneous
459 low-risk HPV8 and MmuPV1 E6 proteins do not target p53 or Notch directly, but bind MAML1, a
460 transcriptional coactivator in the Notch complex, to inhibit Notch activity (25). Indeed, in our study
461 the MmuPV1-E6^{R130A} mutant, which cannot bind to MAML1, failed to show phenotypes such as
462 higher saturation density, inhibition of contact-inhibition/differentiation, or an advantage in the high-
463 density competition assay. In contrast, all of these phenotypes are observed with wild type
464 MmuPV1E6 expression, supporting the idea that the function of MmuPV E6 in the viral life cycle is
465 to give the infected cells a competitive advantage over normal cells primarily by the down regulation
466 of the Notch signalling pathway. Recently published work generated a mouse model carrying an
467 inducible dominant negative mutant of MAML1, which results in inhibition of NICD-induced
468 transcription in the oesophageal keratinocyte cell populations (46). The mutant cells dramatically
469 outcompeted their normal counterparts over time *in vivo*. The persistence of these mutant cells was
470 shown to be due to the MAML1 binding deficient cells not being lost from the basal layer by
471 differentiation, and by their stimulating normal neighbour cells to differentiate. These mutant cell
472 populations also exhibited an increased cell density at 30% confluence, characterised by a resulting
473 buckling of the epithelium (47). Interestingly, we found that HES1 expression, a downstream target of
474 Notch signalling, was not downregulated in MmuPV lesions, and was in fact significantly higher in

475 the basal cells of early lesions when compared to uninfected epithelium (Figure 5). The lesion also
476 appeared to have delayed differentiation where higher HES1 RNA levels were observed. Recent
477 research into the Notch signalling pathway has found that discrete ligand activation of the pathway
478 can have distinct downstream effects. Importantly, it was found that Dll1 and Dll4, two Notch ligands,
479 modulated the Notch receptor in either short frequency-modulated pulses or sustained amplitude-
480 modulated signals respectively. Notch pathway activation by Dll1 led to upregulation of Hes1, whilst
481 Dll4 signalling led to upregulation of Hey1 and HeyL (48). Therefore, we cannot consider Hes1 to be
482 directly representative of a Notch-directed differentiation phenotype in tissue; it appears two discrete
483 pathways can be activated through the Notch receptor. Thorough research into the involvement of
484 Notch in epidermal cell fate has distilled discrete modes of action that Notch signalling activates in
485 spinous cells. Firstly, there can be upregulation of genes required for suprabasal cell differentiation,
486 along with downregulation of genes required to be expressed in the basal layer. In addition, Notch
487 directs maintenance of a proliferative cell phenotype, but can also direct initiation of terminal
488 differentiation. This research showed that Hes1 may in fact be required for maintenance of a
489 proliferative phenotype, and that promotion of differentiation occurs in a Hes1 independent manner
490 (49). It is obvious from our data that the activation of HES1 results from stimulation of a proliferative
491 phenotype in the cells that are also positive for E6/E7 RNA expression. An earlier paper also indicated
492 that upregulation of Hes2 and Hey1 was dependent on a p63 mediated downregulation of Hes1,
493 demonstrating p63 modulation of Notch dependent transcription (50). Overall, it seems that HES1
494 expression in the tissue is indicative of Notch activation, however this is not necessarily a
495 differentiation phenotype and is much more complex than originally thought.

496 The Hippo pathway regulates two transcription factors, YAP/TAZ, and play a central role of sensing
497 the physical and mechanical properties of the microenvironment (cell to cell, and cell to ECM) (51).
498 Hippo also plays a critical role in a wide range of biological processes, including organ size control,
499 cell proliferation, cancer development, and virus-induced diseases (reviewed in (52)). The
500 involvement of the Hippo pathway in the papillomavirus life cycle or pathogenesis has been recently
501 highlighted but little investigated, with literature providing some evidence of it; High-risk HPV E6
502 and HPV8 E6 seem to be targeting and down-regulating the Hippo pathway (53, 54), and the cross

503 talk between YAP/TAZ and the Notch signalling pathway has been reported (41). Further research
504 into this interplay of pathways in the context of virus infection is required to explain the molecular
505 mechanisms of papillomavirus pathogenicity.

506 This work provides evidence of a role for mouse papillomavirus E6 protein in allowing competitive
507 persistence of infected cells at a higher density in the lower layer of monolayer culture, likely
508 mimicking the dynamics of homeostasis in stratified epithelium, especially in the basal layer *in vivo*.

509 MmuPV1 E6 plays a key role, through regulating of the Notch signalling pathway, in the ability of
510 single infected cells to persist in the basal layer of the epithelium over time to allow the establishment
511 of a productive lesion. Disruption of this competitive advantage of lower layer persistence could

512 stimulate the detachment, differentiation and subsequent loss of the infected reservoir of cells,
513 providing a mechanism by which such low-level infection could be treated. If similar mechanisms of
514 persistence are present in papillomaviruses that can cause human disease, therapeutics targeting this

515 pathway could be utilised in tandem with established treatment methods aiming to surgically remove
516 infected cells.

517 **Materials and Methods**

518

519 **Cell culture**

520 Normal immortalized keratinocytes (NIKS) (a gift from Paul Lambert, McArdle Laboratory for
521 Cancer Research, University of Wisconsin) were maintained in FC media with γ -irradiated J2-3T3
522 cells as previously described (38, 55). Mouse primary keratinocytes were isolated from the tail of a
523 nude mouse using Dispase II (Sigma) and trypsin, and then were maintained in FC media with 10 μ M
524 ROCK inhibitor (Y-27632, Generon).

525

526 **Vector construction and retroviral infection**

527 Recombinant retroviruses were produced, and transduction carried out as previously described (56).
528 Construction of the retroviral vectors LXS-N-MmuPV1E6 and MmuPV1E7 was accomplished by
529 cloning the coding sequences utilising Gateway Technology (Thermo Fisher Scientific,
530 Massachusetts, USA) following manufacturer's instructions. The LXS-N-MmuPV1E6^{R130A} mutant was
531 generated using KOD -Plus- Mutagenesis kit (Toyobo, Japan) using primers
532 (AGGCTACTGCGGGTTCTGC and GCCCACATGTGGCGCACC). All constructs generated
533 were sequenced to ensure no additional base changes had occurred. QCXIP-eGFP and QCXIP-
534 mCherry vectors were a gift from Tohru Kiyono, National Cancer Centre, Japan. After transduction,
535 NIKS cells expressing eGFP and mCherry were sorted into four quartiles based on fluorescent
536 intensity using the BD FACSAria Fusion Cell Sorter.

537

538 **Growth and high-density competition assays**

539 In order to represent the growth conditions of the basal layer of stratified epithelium in a 2D *in vitro*
540 assay, cells were seeded at high (confluent) density in a 4-well imaging chamber (MoBiTec,
541 Germany). To each chamber, 2×10^5 of each of NIKS experimental mCherry and eGFP cells were
542 seeded with 4×10^4 irradiated J2-3T3 feeder cells. Cells were cultured for up to 10 days, changing the

543 media every other day, before being fixed in PFA for 10 minutes. Cells were visualised by confocal
544 microscopy (LSM 700, ZEISS, Germany).

545

546 **SDS-PAGE and western blotting**

547 Proteins were extracted from cells using RIPA buffer and quantified using the BCA Protein Assay kit
548 (Pierce, Massachusetts, USA), before being separated on 4–12% gradient polyacrylamide SDS-Tris-
549 Tricine denaturing gel (Invitrogen) and transferred onto PVDF membranes (Bio-Rad). After transfer,
550 membranes were blocked for 1 hour at room temperature in 1% milk in PBS-T (PBS, 0.1% Tween
551 20). Blots were then incubated overnight at 4°C with the appropriate primary antibody diluted in 1%
552 milk in PBS-T. Primary antibodies used were anti-GAPDH (clone MAB374, Millipore,
553 Massachusetts, USA), anti-MAML1 (clone D3E9, Cell Signaling Technology, Massachusetts, USA),
554 and anti-HA (clone ab130275, Abcam, Cambridge, UK). Membranes were then incubated with IR
555 Dye (800CW) fluorescent secondary antibody (LI-COR, Nebraska, USA) for one hour at room
556 temperature, and then washed. Finally, proteins were detected using the Odyssey Imaging System (LI-
557 COR, Nebraska, USA).

558

559 **MmuPV1 preparation**

560 Mus musculus PV type 1 (MmuPV1) was extracted from mouse lesions as previously described (29).
561 Tissue homogenates and cell lysates were incubated at 37°C with Benzonase for 24 h. After a low-
562 speed centrifugation step to remove cellular debris, the virus particles were pelleted by
563 ultracentrifugation then resuspended with PBS + 10% FBS (cell-free virus) (57). Encapsidated virus
564 genome copy number (viral gene equivalent, VGE) was determined by SYBR Green qPCR (Thermo
565 Fisher Scientific, Massachusetts, USA) using type-specific primers
566 (GGTGAGCCTGACCTACCCGA and CGGAGAACAGTGTCGCAGCA).

567

568 **Animal work and ethics**

569 All animal procedures were conducted in accordance with the Animals (Scientific Procedures) Act
570 1986. The protocols were approved by the Animal Welfare and Ethical Review Body (AWERB) of the
571 University of Cambridge and the Home Office (the project licence number: 70/8113). Tails of athymic
572 nude mice (Hsd:Athymic Nude-Foxn1tm, female, 6-8 weeks of age, after a week of acclimatisation;
573 ENVIGO, Indianapolis, United States) or B6 mice (C57BL/6J0laHsd, female, 6-8 weeks of age, after
574 a week of acclimatisation; ENVIGO) were inoculated with 2×10^8 (in 2 μ L volume) of cell-free
575 MmuPV1 following a 3 mm long scarification of the epidermis (up to 3 inoculation sites per tail).
576 Mock infections were carried out with PBS. Tails were harvested after each observation period. Mice
577 were injected intraperitoneally with 200 μ L of 10 mg/mL BrdU (Sigma Aldrich, UK) solution 24 hours
578 before the harvest. For each experimental group, three slides were selected for analysis. For each
579 slide, 7 fields of view were randomly selected.

580

581 **Immunohistochemistry and immunofluorescence**

582 Immunofluorescence and immunohistochemistry were performed as previously described (58). The
583 formalin fixed, paraffin embedded tissue sections were incubated in Target Retrieval Solution, pH 9
584 (Dako, Glostrup, Denmark) for 10 min at room temperature prior to incubating for 15 min at 110°C.
585 The cells were washed in PBS and fixed in 4% paraformaldehyde (PFA) in PBS for 10 min at room
586 temperature. The cells were permeabilised in PBS with 0.1% Triton X-100 (Promega) for 30 min,
587 then washed in PBS. The sections and cells were blocked in 10% normal goat serum in PBS for 1
588 hour prior to incubation with the primary antibodies. The antibodies used were an in-house rabbit anti-
589 MmuPV1 E4 and L1 monoclonal antibodies (29), mouse anti-DE-K10 (Invitrogen, CA), rat anti-
590 BrdU, and rabbit anti-Cytokeratin 17 (Abcam, Cambridge, UK). Antigen antibody complexes were
591 visualised with an anti-mouse Alexa 488- or 594-conjugated antibody (Thermo Fisher Scientific).
592 Nuclei were visualised with DAPI. BrdU and K10 positive cells were counted manually.

593

594 **RNA *in situ* hybridisation**

595 Viral transcripts cells were detected and visualised using RNAScope In Situ Hybridization Assay

596 (Advanced Cell Diagnostics, Minnesota, United States) following manufacturer's instructions. The
597 probe used for MmPV1 RNA detection was MusPV-E6-E7 (Cat No. 409771), and the probe used for
598 HES1 RNA was Mm-Hes1-C2 (Cat No. 417701-C2).

599 **Acknowledgments**

600 This work is supported by the Medical Research Council (MC-PC-13050 and MR/S024409/1) and
601 the Department of Pathology, University of Cambridge. We would also like to acknowledge the
602 Addenbrooke's Hospital Tissue Bank facility for the sectioning and embedding of tissue samples and
603 the IMS-MRL Imaging Core for image analysis, (Wellcome Trust Major Award 208363/Z/17/Z). We
604 would also like to acknowledge Adeline Nicholas for proofreading the manuscript. Finally, we would
605 like to thank Professor Neil Christensen for his generous gift of the MmuPV1 sample.

606

607 **References**

- 608 1. Egawa N, Doorbar J. 2017. The low-risk papillomaviruses. *Virus Res* 231:119-127.
- 609 2. Van Doorslaer K. 2013. Evolution of the papillomaviridae. *Virology* 445:11-20.
- 610 3. Ingle A, Ghim S, Joh J, Chepkoech I, Bennett Jenson A, Sundberg JP. 2011. Novel
611 laboratory mouse papillomavirus (MusPV) infection. *Vet Pathol* 48:500-5.
- 612 4. Joh J, Jenson AB, King W, Proctor M, Ingle A, Sundberg JP, Ghim SJ. 2011. Genomic
613 analysis of the first laboratory-mouse papillomavirus. *J Gen Virol* 92:692-8.
- 614 5. Cladel NM, Budgeon LR, Balogh KK, Cooper TK, Hu J, Christensen ND. 2016. Mouse
615 papillomavirus MmuPV1 infects oral mucosa and preferentially targets the base of
616 the tongue. *Virology* 488:73-80.
- 617 6. Cladel NM, Budgeon LR, Balogh KK, Cooper TK, Hu J, Christensen ND. 2015. A novel
618 pre-clinical murine model to study the life cycle and progression of cervical and anal
619 papillomavirus infections. *PLoS One* 10:e0120128.
- 620 7. Hu J, Budgeon LR, Cladel NM, Balogh K, Myers R, Cooper TK, Christensen ND. 2015.
621 Tracking vaginal, anal and oral infection in a mouse papillomavirus infection model. *J*
622 *Gen Virol* 96:pp3554-3565.
- 623 8. Spurgeon ME, Uberoi A, McGregor SM, Wei T, Ward-Shaw E, Lambert PF. 2019. A
624 Novel In Vivo Infection Model To Study Papillomavirus-Mediated Disease of the
625 Female Reproductive Tract. *mBio* 10.
- 626 9. Handisurya A, Day PM, Thompson CD, Buck CB, Pang YY, Lowy DR, Schiller JT. 2013.
627 Characterization of *Mus musculus* papillomavirus 1 infection in situ reveals an
628 unusual pattern of late gene expression and capsid protein localization. *J Virol*
629 87:13214-25.
- 630 10. Shafti-Keramat S, Handisurya A, Kriehuber E, Meneguzzi G, Slupetzky K, Kirnbauer R.
631 2003. Different heparan sulfate proteoglycans serve as cellular receptors for human
632 papillomaviruses. *J Virol* 77:13125-35.
- 633 11. Wang JW, Jiang R, Peng S, Chang YN, Hung CF, Roden RB. 2015. Immunologic Control
634 of *Mus musculus* Papillomavirus Type 1. *PLoS Pathog* 11:e1005243.
- 635 12. Uberoi A, Yoshida S, Frazer IH, Pitot HC, Lambert PF. 2016. Role of Ultraviolet
636 Radiation in Papillomavirus-Induced Disease. *PLoS Pathog* 12:e1005664.
- 637 13. Hu J, Cladel NM, Budgeon LR, Balogh KK, Christensen ND. 2017. The Mouse
638 Papillomavirus Infection Model. *Viruses* 9.
- 639 14. Egawa N, Egawa K, Griffin H, Doorbar J. 2015. Human Papillomaviruses; Epithelial
640 Tropisms, and the Development of Neoplasia. *Viruses* 7:3863-90.
- 641 15. Sichero L, Rollison DE, Amorrortu RP, Tommasino M. 2019. Beta Human
642 Papillomavirus and Associated Diseases. *Acta Cytol* 63:pp100-108.
- 643 16. Jablonska S, Dabrowski J, Jakubowicz K. 1972. Epidermodysplasia verruciformis as a
644 model in studies on the role of papovaviruses in oncogenesis. *Cancer Res* 32:583-9.
- 645 17. Bouvard V, Baan R, Straif K, Grosse Y, Secretan B, El Ghissassi F, Benbrahim-Tallaa L,
646 Guha N, Freeman C, Galichet L, Coglianò V. 2009. A review of human carcinogens--
647 Part B: biological agents. *The lancet oncology* 10:321-2.
- 648 18. Doorbar J, Quint W, Banks L, Bravo IG, Stoler M, Broker TR, Stanley MA. 2012. The
649 biology and life-cycle of human papillomaviruses. *Vaccine* 30 Suppl 5:F55-70.
- 650 19. Potten CS, Saffhill, R., Maibach, H.I. 1987. Measurement of the transit time for cells
651 through the epidermis and stratum corneum of the mouse and guinea-pig. *Cell*
652 *Tissue Kinetics* 20:pp461-472.

- 653 20. Potten CS. 1981. Cell replacement in epidermis (keratopoiesis) via discrete units of
654 proliferation. *Int Rev Cytol* 69:271-318.
- 655 21. Doupe DP, Klein AM, Simons BD, Jones PH. 2010. The ordered architecture of murine
656 ear epidermis is maintained by progenitor cells with random fate. *Dev Cell* 18:pp317-
657 323.
- 658 22. Roshan A, Murai K, Fowler J, Simons BD, Nikolaidou-Neokosmidou V, Jones PH. 2016.
659 Human keratinocytes have two interconvertible modes of proliferation. *Nat Cell Biol*
660 18:pp145-156.
- 661 23. Hufbauer M, Biddle A, Borgogna C, Gariglio M, Doorbar J, Storey A, Pfister H,
662 Mackenzie I, Akgul B. 2013. Expression of betapapillomavirus oncogenes increases
663 the number of keratinocytes with stem cell-like properties. *J Virol* 87:12158-65.
- 664 24. Kranjec C, Holleywood C, Libert D, Griffin H, Mahmood R, Isaacson E, Doorbar J.
665 2017. Modulation of basal cell fate during productive and transforming HPV-16
666 infection is mediated by progressive E6-driven depletion of Notch. *J Pathol* 242:448-
667 462.
- 668 25. Meyers JM, Uberoi A, Grace M, Lambert PF, Munger K. 2017. Cutaneous HPV8 and
669 MmuPV1 E6 Proteins Target the NOTCH and TGF-beta Tumor Suppressors to Inhibit
670 Differentiation and Sustain Keratinocyte Proliferation. *PLoS Pathog* 13:e1006171.
- 671 26. Rangarajan A, Talora C, Okuyama R, Nicolas M, Mammucari C, Oh H, Aster JC, Krishna
672 S, Metzger D, Chambon P, Miele L, Aguet M, Radtke F, Dotto GP. 2001. Notch
673 signaling is a direct determinant of keratinocyte growth arrest and entry into
674 differentiation. *EMBO Journal* 20:pp3427-3436.
- 675 27. Lin HY, Kao CH, Lin KM, Kaartinen V, Yang LT. 2011. Notch signaling regulates late-
676 stage epidermal differentiation and maintains postnatal hair cycle homeostasis. *PLoS*
677 *One* 6:e15842.
- 678 28. Blanpain C, Lowry WE, Pasolli HA, Fuchs E. 2006. Canonical notch signaling functions
679 as a commitment switch in the epidermal lineage. *Genes Dev* 20:pp3022-3035.
- 680 29. Egawa N, Shiraz A, Crawford R, Saunders-Wood T, Yarwood J, Rogers M, Sharma A,
681 Eichenbaum G, Doorbar J. 2021. Dynamics of papillomavirus in vivo disease
682 formation & susceptibility to high-level disinfection-Implications for transmission in
683 clinical settings. *EBioMedicine* 63:103177.
- 684 30. Freedberg IM, Tomic-Canic M, Komine M, Blumenberg M. 2001. Keratins and the
685 keratinocyte activation cycle. *J Invest Dermatol* 116:633-40.
- 686 31. Stanley MA. 2012. Epithelial cell responses to infection with human papillomavirus.
687 *Clinical microbiology reviews* 25:215-22.
- 688 32. Noble R. 1979. Sexually Transmitted Disease: Guide to Diagnosis and Therapy.:112-
689 117.
- 690 33. Pfister H. 1987. Relationship of papillomaviruses to anogenital cancer. *Obstet*
691 *Gynecol Clin North Am* 14:349-61.
- 692 34. Amoyel M, Bach EA. 2014. Cell competition: how to eliminate your neighbours.
693 *Development* 141:988-1000.
- 694 35. Kranjec C, Doorbar J. 2016. Human papillomavirus infection and induction of
695 neoplasia: a matter of fitness. *Curr Opin Virol* 20:129-136.
- 696 36. Sundberg JP, Stearns TM, Joh J, Proctor M, Ingle A, Silva KA, Dadras SS, Jenson AB,
697 Ghim SJ. 2014. Immune status, strain background, and anatomic site of inoculation
698 affect mouse papillomavirus (MmuPV1) induction of exophytic papillomas or
699 endophytic trichoblastomas. *PLoS One* 9:e113582.

- 700 37. Cladel NM, Budgeon LR, Balogh KK, Cooper TK, Brendle SA, Christensen ND, Schell
701 TD, Hu J. 2017. Mouse papillomavirus infection persists in mucosal tissues of an
702 immunocompetent mouse strain and progresses to cancer. *Sci Rep* 7.
- 703 38. Murakami I, Egawa N, Griffin H, Yin W, Kranjec C, Nakahara T, Kiyono T, Doorbar J.
704 2019. Roles for E1-independent replication and E6-mediated p53 degradation during
705 low-risk and high-risk human papillomavirus genome maintenance. *PLoS Pathog*
706 15:e1007755.
- 707 39. Uberoi A, Lambert PF. 2017. Rodent Papillomaviruses. *Viruses* 9.
- 708 40. Macara IG, Guyer R, Richardson G, Huo Y, Ahmed SM. 2014. Epithelial homeostasis.
709 *Curr Biol* 24:R815-25.
- 710 41. Totaro A, Castellan M, Di Biagio D, Piccolo S. 2018. Crosstalk between YAP/TAZ and
711 Notch Signaling. *Trends Cell Biol* 28:560-573.
- 712 42. Hsu YC, Li L, Fuchs E. 2014. Emerging interactions between skin stem cells and their
713 niches. *Nat Med* 20:pp847-856.
- 714 43. Nowell C, Radtke F. 2013. Cutaneous Notch signaling in health and disease. *Cold*
715 *Spring Harb Perspect Med* 3:a017772.
- 716 44. Siebel C, Lendahl U. 2017. Notch Signaling in Development, Tissue Homeostasis, and
717 Disease. *Physiol Rev* 97:1235-1294.
- 718 45. Yugawa T, Handa K, Narisawa-Saito M, Ohno S, Fujita M, Kiyono T. 2007. Regulation
719 of Notch1 gene expression by p53 in epithelial cells. *Mol Cell Biol* 27:3732-42.
- 720 46. Alcolea MP, Jones PH. 2015. Cell competition: winning out by losing notch. *Cell Cycle*
721 14:pp9-17.
- 722 47. Alcolea MP, Greulich P, Wabik A, Frede J, Simons BD, Jones PH. 2014. Differentiation
723 imbalance in single oesophageal progenitor cells causes clonal immortalization and
724 field change. *Nat Cell Biol* 16:pp615-622.
- 725 48. Nandagopal N, Santat LA, LeBon L, Sprinzak D, Bronner ME, Elowitz MB. 2018.
726 Dynamic Ligand Discrimination in the Notch Signaling Pathway. *Cell* 172:869-880.e19.
- 727 49. Moriyama M, Durham AD, Moriyama H, Hasegawa K, Nishikawa S, Radtke F, Osawa
728 M. 2008. Multiple roles of Notch signaling in the regulation of epidermal
729 development. *Dev Cell* 14:594-604.
- 730 50. Nguyen BC, Lefort K, Mandinova A, Antonini D, Devgan V, Della Gatta G, Koster MI,
731 Zhang Z, Wang J, Tommasi di Vignano A, Kitajewski J, Chiorino G, Roop DR, Missero C,
732 Dotto GP. 2006. Cross-regulation between Notch and p63 in keratinocyte
733 commitment
734 to differentiation. *Genes and Development* 20:pp1028-1042.
- 735 51. Panciera T, Azzolin L, Cordenonsi M, Piccolo S. 2017. Mechanobiology of YAP and TAZ
736 in physiology and disease. *Nat Rev Mol Cell Biol* 18:758-770.
- 737 52. Wang Z, Lu W, Zhang Y, Zou F, Jin Z, Zhao T. 2019. The Hippo Pathway and Viral
738 Infections. *Front Microbiol* 10:3033.
- 739 53. Dacus D, Cotton C, McCallister TX, Wallace NA. 2020. Beta Human Papillomavirus 8E6
740 Attenuates LATS Phosphorylation after Failed Cytokinesis. *J Virol* 94.
- 741 54. Webb Strickland S, Brimer N, Lyons C, Vande Pol SB. 2018. Human Papillomavirus E6
742 interaction with cellular PDZ domain proteins modulates YAP nuclear localization.
743 *Virology* 516:127-138.
- 744 55. Flores ER, Allen-Hoffmann BL, Lee D, Sattler CA, Lambert PF. 1999. Establishment of
745 the human papillomavirus type 16 (HPV-16) life cycle in an immortalized human
746 foreskin keratinocyte cell line. *Virology* 262:344-54.

- 747 56. Naviaux RK, Costanzi E, Haas M, Verma IM. 1996. The pCL vector system: rapid
748 production of helper-free, high-titer, recombinant retroviruses. *J Virol* 70:5701-5.
- 749 57. Ozbun MA, Patterson NA. 2014. Using organotypic (raft) epithelial tissue cultures for
750 the biosynthesis and isolation of infectious human papillomaviruses. *Curr Protoc*
751 *Microbiol* 34:14B 3 1-18.
- 752 58. Wang Q, Griffin H, Southern S, Jackson D, Martin A, McIntosh P, Davy C, Masterson
753 PJ, Walker PA, Laskey P, Omary MB, Doorbar J. 2004. Functional analysis of the
754 human papillomavirus type 16 E1^{E4} protein provides a mechanism for in vivo and in
755 vitro keratin filament reorganization. *Journal of Virology* 78:821-33.
- 756
- 757

758 **Figure legends**

759

760 **Figure 1. Spatial localisation of MmuPV1 E6/E7 expression, E4 and L1 protein in early lesion**
761 **formation of infected tissues**

762 (A-D) Time course analysis of early lesion formation of sites infected with MmuPV1 cell-free virus.
763 Each set of panels shows H&E staining (top), E6/E7 RNAScope signal (middle), and
764 immunofluorescent detection of E4 and L1 proteins (bottom) at a discrete stage of lesion formation.
765 Staining was carried out on adjacent sections. The nuclei were counter-stained with DAPI. The scale
766 is shown with a white bar (100 μ m). The boxed areas are enlarged at the bottom (A and B). The dotted
767 lines indicate the position of the basal layer.

768

769 **Figure 2. Identification of productive MmuPV1 lesions in immunocompetent mice**

770 (A) Diagrammatic representation of inoculation site procedure in our model (left panel). Inoculation
771 sites are shown in red, and the 1 cm spaces between the centre of each wound site are annotated. The
772 first wound site is located 1 cm down from the base of the tail. Early visible lesion formation on
773 immunodeficient Nude mouse tail 10 days post infection, sites indicated with red line (centre panel).
774 C57BL/6 immunocompetent mice showed no evidence of papilloma formation at wound sites 10 days
775 post infection (right panel). (B) Transient lesions located in C57BL/6 immunocompetent mouse tail
776 tissue wound site 7 and 10 days following inoculation (i and ii). Panels show H&E staining (top
777 panel), E6/E7 RNAScope immunofluorescence and E4 protein (centre), and immunofluorescent
778 detection of E4 and L1 proteins (bottom panel). The nuclei were counter-stained with DAPI. The
779 scale is shown with a white bar (100 μ m). The boxed areas in H&E staining are enlarged. The dotted
780 lines indicate the position of the basal layer.

781

782 **Figure 3. Differences in basal cell density and DNA replication in developing lesions**

783 (A) Representative images of four categories, uninfected epithelium, mock wound sites, early visible
784 lesions in nude mouse (samples collected 6 or 7 days post infection, validated using E6/E7
785 RNAScope), and established lesions (samples collected from tail lesions more than 10 days post-

786 infection), of tissue are shown. Infected lesion was identified by E4 expression, and wounded area
787 was identified by K17 expression. The nuclei were counter-stained with DAPI. The white dotted lines
788 indicate location of basement membranes, and red dotted line indicates the areas which were
789 measured. The scale is shown with a white bar (200 μm). (B) Basal cell density was quantified by
790 measuring 450 μm stretches of epithelium in 40 image sets taken from different nude mice (n=4 per
791 category). P-values were calculated with Kruskal-Wallis test with Dunn's correction. (C)
792 Representative images are shown (right panel) for each category. Proliferating cells were visualised
793 by BrdU staining. The nuclei were counter-stained with DAPI. White dotted lines indicate location of
794 basement membranes. The scale is shown with a white bar (50 μm). (D) The percentage of BrdU
795 positive cells in the basal layer of the above four categories (n=3). P-values were calculated with
796 Kruskal-Wallis test with Dunn's correction.

797

798 **Figure 4. Heterogeneous expression pattern of E6/E7 RNA in the basal layer.**

799 (A) Representative images of viral E6/E7 RNAScope in the early visible lesion. The dotted lines
800 indicate location of basement membranes. The scale is shown with a white bar (50 μm). (B)
801 Distribution of viral RNA expression levels in basal cells of early visible lesions (n=4) is shown in the
802 histogram. Intensity of expression per cell (AU) is grouped into bin centres for bimodal analysis. A
803 Sum of Two Lorentzian distribution line is fit to the data (Red).

804

805 **Figure 5. Delay in normal differentiation induction occurs in tissue in E6/E7 RNA positive cells**

806 (A and B) An early visible lesion from a nude mouse was stained for K10 (red), E6E7 RNAScope (A)
807 or HES-1 RNAScope (B) (green) and nuclei with DAPI (blue). The dotted lines indicate the position
808 of the basal layer. The yellow boxed area is enlarged at the bottom. Scale bar: 100 μm . (C) A
809 microlesion from a C57BL/6 mouse (Figure 2B-i) stained for K10 (red), HES-1 RNAScope (green)
810 and nuclei with DAPI (blue). The dotted lines indicate the position of the basal layer. The yellow
811 boxed area is enlarged at the bottom. Scale bar: 100 μm . (D) An uninfected epithelium (top) and an
812 infected lesion (bottom) were stained for HES-1 RNAScope (green) and DAPI (blue). The dotted

813 lines indicate the position of the basal layer. Scale bar: 100 μm . (E) Box plot to show intensity of
814 HES-1 RNA expression in the basal layer of cells of uninfected epithelium (n=10) and lesion (n=10).
815 P-values were calculated with a Kolmogorov-Smirnov t-test; **** = $P \leq 0.0001$.

816

817 **Figure 6. Exogenous expression of MmuPV1 E6 leads to higher cell density and differentiation**
818 **delay in keratinocytes**

819 (A) NIKS/LXSN, or NIKS expressing MmuPV1 E6 or E7, were counted in triplicate every day. Cells
820 were confluent around day 4. P-values were calculated with a two-way ANOVA with Tukey's
821 correction; **** = $P \leq 0.0001$. (B) Cells were stained with K10 (red) and DAPI (blue) at both pre-
822 confluence (day 3) and post-confluence (day 7). Scale bar: 100 μm . Light microscope images for each
823 time point are also shown. Red arrows denote presence of ring-like structures in cell monolayer
824 morphology. Black arrows denote the presence of bright, rounded cells. (C) Number of K10 positive
825 cells per field for each cell population. P-values were calculated with Kruskal-Wallis test with Dunn's
826 correction; * = $P \leq 0.05$.

827

828 **Figure 7. NIKS expressing MmuPV1 E6 preferentially persist in the lower layer of cells in a**
829 **high-density competition assay**

830 (A) NIKS cells were seeded at high density and cultured for 7 days. 3D image of NIKS cells at day 7
831 stained with K14 and K10 is shown. (B) The same number of each cell line was seeded together at
832 day 0, and the proportions of each cell lines of each group LXSN(green)/LXSN(red),
833 LXSN(green)/LXSN-MmuPV1E6(red), and LXSN(green)/LXSN-MmuPV1E7(red), at day 1 are
834 shown. (C and D) Representative images of lower layer (C) and upper layer (D) of each group are
835 shown (left), alongside the proportions of each cell lines of each group (right) at day 10. Experimental
836 groups were compared with LXSN/LXSN control groups, and P-values were calculated with a two-
837 way ANOVA with Sidak's multiple comparisons test. NS: not significant. Scale bar: 100 μm . (E)
838 Maximum intensity 3D plots of z-stacks are shown for each of the three groups. Annotations show the

839 location of the lower and upper layers. White dotted lines indicate the bottom of the slide glass on
840 which the cells are cultured. The nuclei were counter-stained with DAPI.

841 **Figure 8. Viral protein expression can alter cell density of the ‘lower’ layer of cells**

842 Quantification of the number of cells in the bottom layer of each population (field size:
843 800.22x800.22 mm). Five random 5 by 5 tile scans were chosen for quantification for each group at a
844 day 7 timepoint. P-values were calculated with Kolmogorov-Smirnov t-tests; ** = $P \leq 0.01$.

845

846 **Figure 9. MmuPV1 E6 interaction with MAML1 is required for post-confluent density increase
847 and differentiation delay**

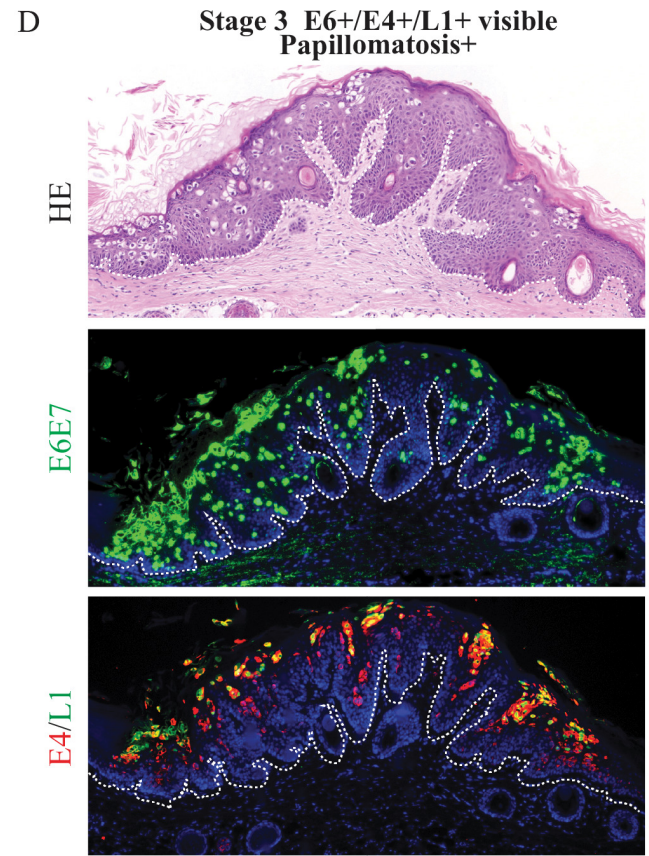
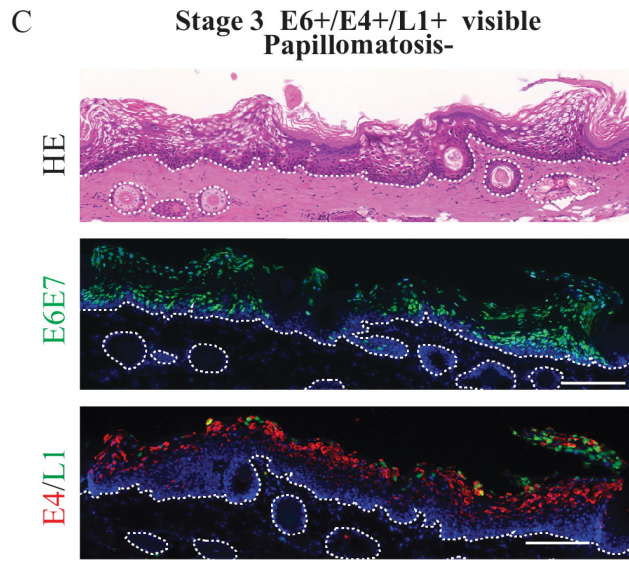
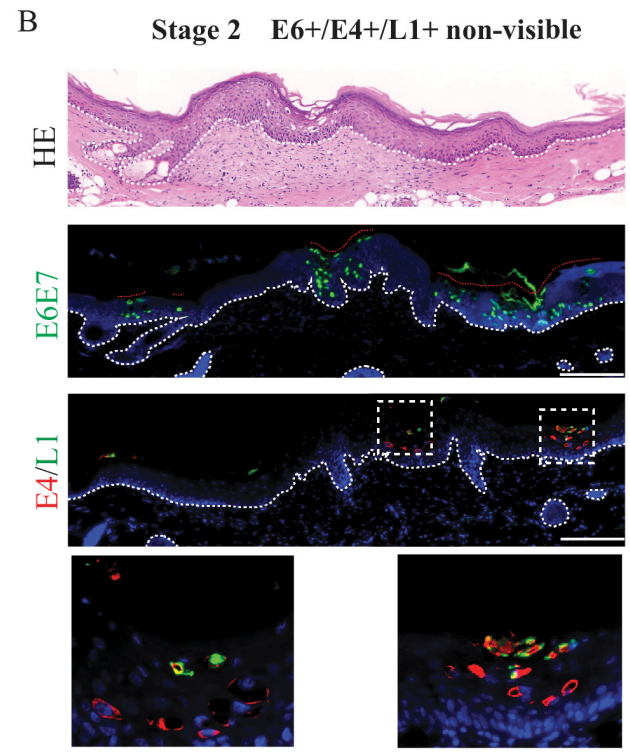
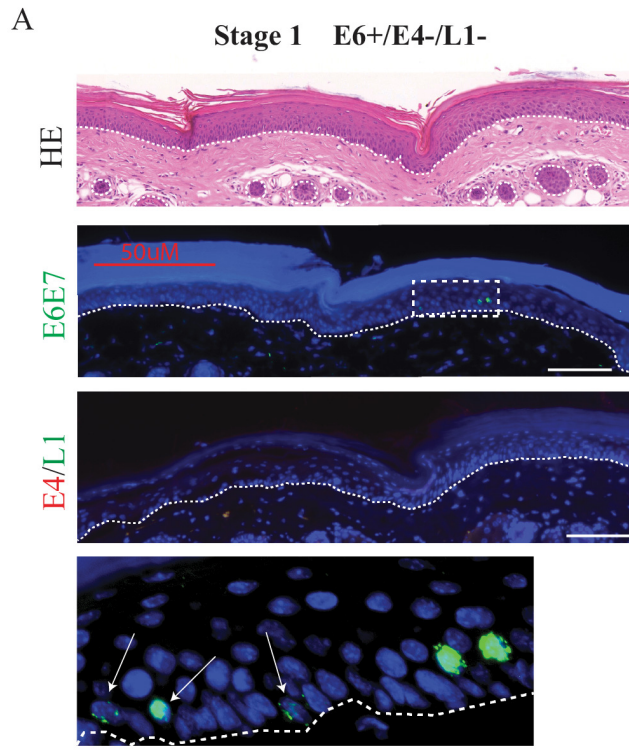
848 (A) Lysates of 293TT cells expressing HA-tagged wild-type or mutant MmuPV1 E6 protein were
849 subjected to an immunoprecipitation using HA antibody. Immunoprecipitated MmuPV1 E6 and
850 associated MAML1 detected by immunoblotting. Expression levels of proteins were assessed by
851 immunoblotting of total cell lysate (TCL). GAPDH expression was used as a loading control. (B)
852 NIKS/LXSN, NIKS/LXSN-MmuPV1E6 or NIKS/LXSN-MmuPV1E6^{R130A} cells were counted each
853 day. Cells were confluent around day 4. P-values were calculated with a two-way ANOVA with
854 Tukey’s correction; **** = $P \leq 0.0001$. (C) NIKS/LXSN, NIKS/LXSN-MmuPV1E6 or NIKS/LXSN-
855 MmuPV1E6^{R130A} cells were stained with K10 (red) at both pre-confluence (day 3) and post-
856 confluence (day 7). Nuclei were counterstained with DAPI. Scale bar: 100 μ m. Light microscope
857 images for each time point are also shown for all three cell populations. Red arrows denote presence
858 of ring-like structures in cell monolayer morphology. (D) Number of K10 positive cells per field for
859 NIKS/LXSN-MmuPV1E6 or NIKS/LXSN-MmuPV1E6^{R130A} cells. P-values were calculated with
860 Kruskal-Wallis test with Dunn’s correction; * = $P \leq 0.05$.

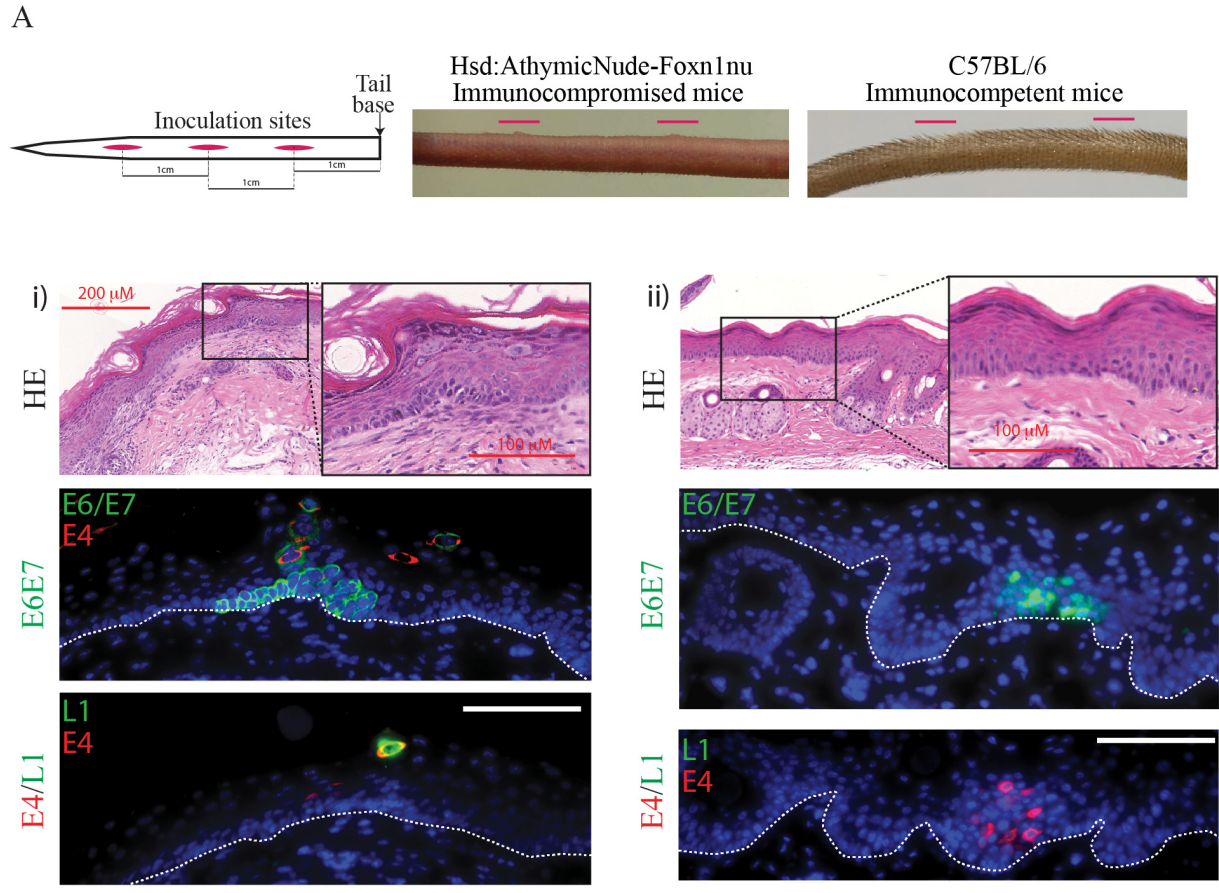
861

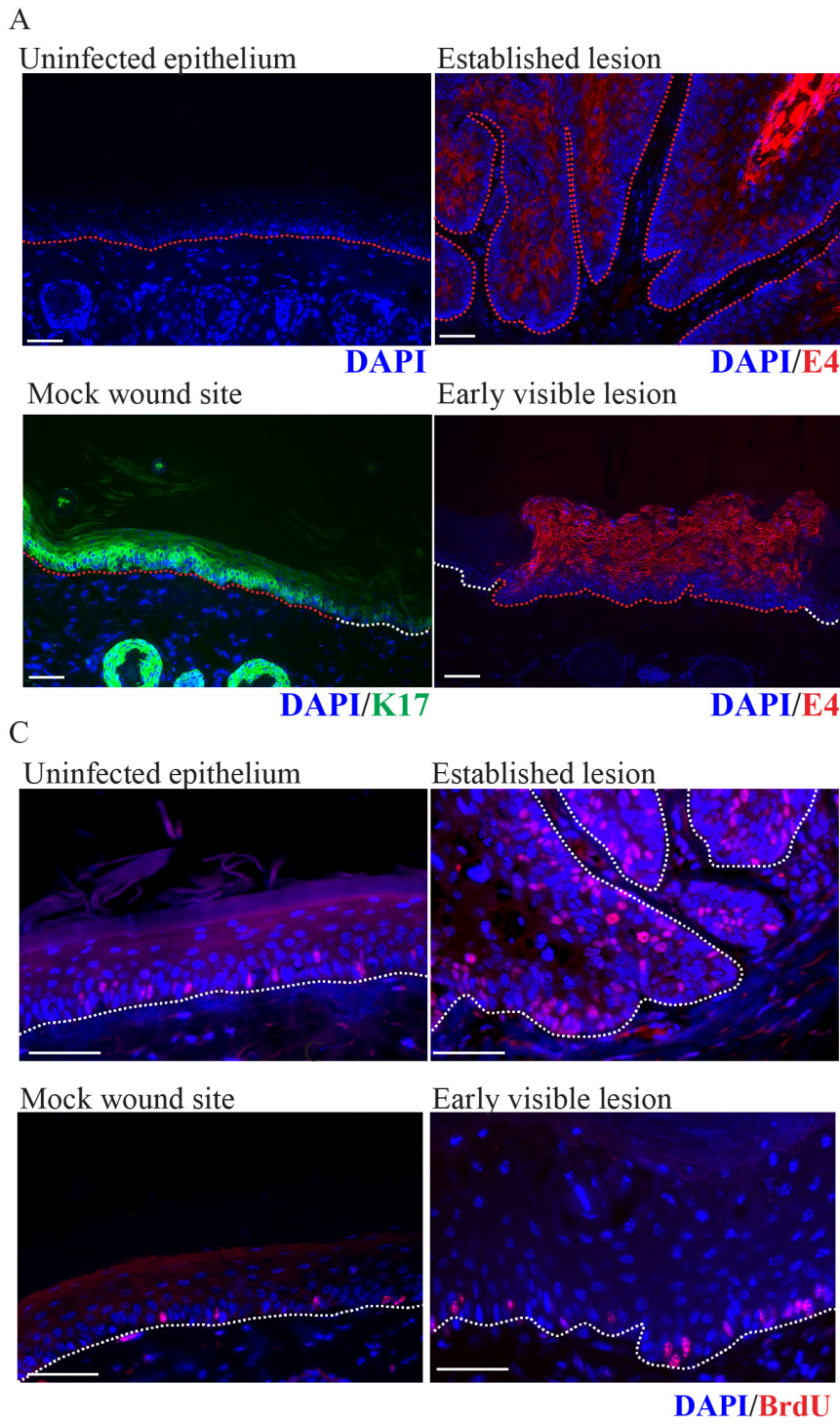
862 **Figure 10. MmuPV1 E6 interaction with MAML1 is required for preferential persistence in the
863 lower layer of cells in high-density competition assay**

864 (A and B) Representative images of lower layer (A) and upper layer (B) of each group are shown
865 (left), alongside the proportions of each cell lines of each group (right). Experimental groups were

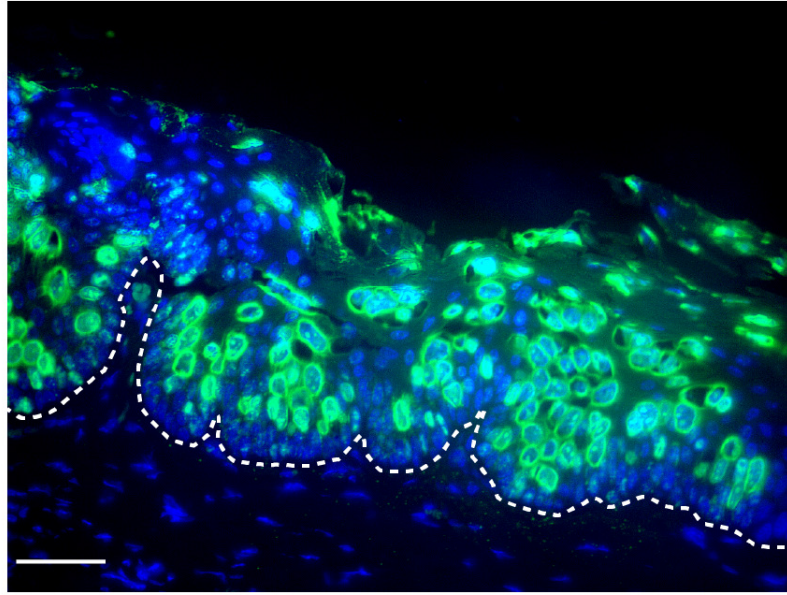
866 compared each other, and P-values were calculated with a two-way ANOVA with Sidak's multiple
867 comparisons test. NS: not significant. Scale bar: 100 μm . (C) Maximum intensity 3D plots of z-stacks
868 are shown for each group. Annotations show the location of the lower and upper layers. White dotted
869 lines indicate the bottom of the slide glass on which the cells are cultured. The nuclei were counter-
870 stained with DAPI. (D) Quantification of the number of cells in the bottom layer of each population
871 (field size: 800.22x800.22 μm). Five random 5 by 5 tile scans were chosen for quantification for each
872 group at a day 7 timepoint. P-values were calculated with Kolmogorov-Smirnov t-tests; ** = $P \leq 0.01$.
873 NS: not significant.







A



DAPI/E6E7

B

